[natY/90Y]Yttrium and [natLu/177Lu]Lutetium Complexation by Rigid H4OCTAPA Derivatives. Effect of Ligand Topology

Fátima Lucio-Martínez, Balazs Szilagyi, Rocío Uzal-Varela, Paulo Perez-Lourido, David Esteban-Gómez, Nicolas Lepareur, Gyula Tircsó, Carlos Platas-Iglesias

Chemistry–A European Journal

Research Article
doi.org/10.1002/chem.202500799

Chemistry Europe
European Chemical Societies Publishing

www.chemeurj.org

[^{nat}Y/^{90}Y]Yttrium and [^{nat}Lu/^{177}Lu]Lutetium Complexation by Rigid H_4OCTAPA Derivatives. Effect of Ligand Topology

Fátima Lucio-Martínez,[a] Balázs Szilágyi,[b, c] Rocío Uzal-Varela,[a] Paulo Pérez-Lourido,[d] David Esteban-Gómez,[a] Nicolas Lepareur,[e] Gyula Tircsó,*[b] and Carlos Platas-Iglesias*[a]

We present a detailed investigation on the coordination chemistry of [$^{nat/90}$Y]Y^{3+} and [$^{nat/177}$Lu]Lu^{3+} with the new acyclic chelator H_4*CHX*OITAPA. This octadentate chelator forms nine-coordinated Y^{3+} and Lu^{3+} complexes thanks to the coordination of a water molecule, as demonstrated by the X-ray structure of [Y(H*CHX*OITAPA)(H_2O)] and ^{1}H, ^{13}C, and ^{89}Y NMR studies in solution. These complexes display slightly higher thermodynamic stabilities compared with those of the known H_4*CHX*OCTAPA and H_4OCTAPA chelators, reaching log K_{YL} and log K_{LuL} values of 21.24(5) and 21.96(1), respectively. Kinetic studies indicate that these complexes dissociate mainly through the spontaneous and proton-assisted pathways at pH 7.4. The chelator can be readily radiolabeled with [^{90}Y]Y^{3+} and [^{177}Lu]Lu^{3+} at room temperature in 10 min. The radio-complexes are stable in human serum at 37 °C, in contrast with the analogues of the known H_4*CHX*OCTAPA and H_4OCTAPA chelators, which experience significant dissociation under these conditions. Thus, the H_4*CHX*OITAPA chelator represents the most promising candidate among the H_4OCTAPA family for the development of ^{90}Y- and ^{177}Lu-based radiopharmaceuticals.

1. Introduction

The H_4OCTAPA ligand and its derivatives (Figure 1) have emerged as a very interesting platform for the complexation of large metal ions such as the lanthanide ions (Ln^{3+}), In^{3+}, and Bi^{3+}. This ligand was initially designed for Gd^{3+} complexation as a potential contrast agent (CA) for magnetic resonance imaging (MRI),[1] as its octadentate nature provides a coordination position available for a water molecule, as confirmed by the X-ray structure of the complex[2] and luminescence measurements on the Eu^{3+} and Tb^{3+} chelates.[1,3] After these initial studies, H_4OCTAPA was not investigated further for some time, probably because of the low thermodynamic stability of the Gd^{3+} complex estimated initially.[2] A renewed interest in this ligand arose after the discovery of its excellent properties for In^{3+} complexation, making H_4OCTAPA an ideal candidate for [^{111}In]Indium-based radiopharmaceuticals for imaging using single photon emission computed tomography (SPECT).[4] Subsequent studies showed that H_4OCTAPA forms highly stable complexes with the Cu^{2+} and Ln^{3+} ions,[5,6] though dissociation kinetics were found to be fast.[5]

Several structural modifications were introduced to improve the inertness of OCTAPA complexes. For instance, the incorporation of a rigid cyclohexyl ring to give H_4*CHX*OCTAPA increases notably the inertness of the lanthanide complexes,[7] without compromising thermodynamic stability. This ligand also showed enhanced affinity for In^{3+} compared to the more flexible H_4OCTAPA.[8] Recently, we also reported the rigid cyclopentyl derivative H_4CpOCTAPA, but its properties were found to be inferior to those of H_4*CHX*OCTAPA in [$^{205/206}$Bi]Bi radiolabelling experiments.[9]

Some Ln^{3+} ions, as well as Y^{3+}, have very attractive properties for application as radiopharmaceuticals.[10–12] Indeed, the ^{177}Lu- and ^{90}Y-nuclides are β^- emitters with half-lives of ≈6.6 and 2.7 days, respectively, which makes them very useful for therapeutic purposes. The high β^- emission energy of the ^{90}Y-nuclide (2290 keV)[13] makes it particularly appropriate to treat large tumours with poor vascularization. This confers to the ^{90}Y-nuclide a large β^- range in vivo of up to 12 mm, which represents a 6-fold increase with respect to the ^{177}Lu-nuclide (β^- emission energy of 498 keV). Conversely, the relatively small penetration of β^- particles emitted by the ^{177}Lu-nuclide makes it

[a] Dr. F. Lucio-Martínez, Dr. R. Uzal-Varela, Prof. Dr. D. Esteban-Gómez, Prof. Dr. C. Platas-Iglesias
Centro Interdisciplinar de Química e Bioloxía and Departamento de Química, Universidade da Coruña, Campus da Zapateira-Rúa da Fraga 10, A Coruña 15001, Spain
E-mail: carlos.platas.iglesias@udc.es

[b] B. Szilágyi, Prof. Dr. G. Tircsó
Department of Physical Chemistry, University of Debrecen, Debrecen H-4010, Hungary
E-mail: gyula.tircso@science.unideb.hu

[c] B. Szilágyi
Doctoral School of Chemistry, Faculty of Science and Technology, University of Debrecen, Debrecen H-4010, Hungary

[d] Prof. Dr. P. Pérez-Lourido
Departamento de Química Inorgánica, Facultad de Ciencias, Universidade de Vigo, As Lagoas, Marcosende, Pontevedra 36310, Spain

[e] Dr. N. Lepareur
Centre Eugène Marquis, Inrae, Inserm, Institut NUMECAN (Nutrition, Métabolismes et Cancer), University of Rennes, UMR_A 1341, UMR_S 1317, Rennes F-35000, France

Supporting information for this article is available on the WWW under https://doi.org/10.1002/chem.202500799

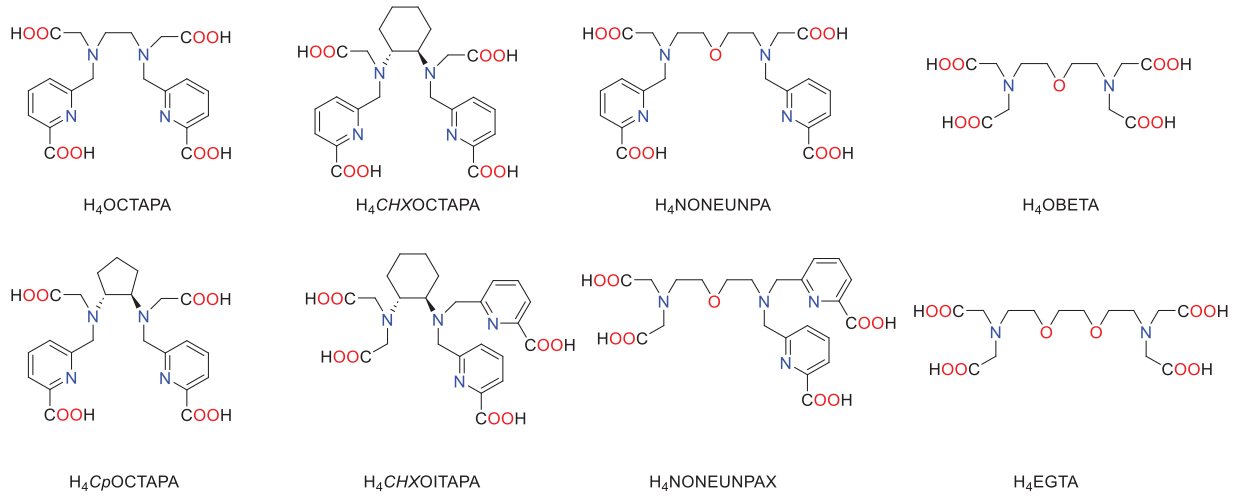

Figure 1. Structures of ligands are discussed in the present work.

very well suited to treat small tumors, including micrometastatic disease.[14] The coordination chemistry of Y^{3+} and Lu^{3+} is very much similar, and thus one can reasonably use the same chelator for the design of ^{177}Lu- and ^{90}Y-based radiopharmaceuticals. Several ^{177}Lu- and ^{90}Y-based radiopharmaceuticals (Lutathera, Pluvicto, etc.) are already used in clinical practice,[15–17] and many others are currently undergoing clinical trials.[18] The properties of the chelator may affect those of the bifunctional derivative used in therapy, and thus developing new chelators for this application is very important.

We have recently reported a detailed study of the structure and dissociation kinetics of the Ln^{3+} complexes of H$_4$*CHX*OCTAPA across the lanthanide series.[3] This study revealed an unexpected behavior, as the dissociation of the complexes with the heaviest Ln^{3+} ions at physiological pH is dominated by the metal-assisted mechanism (in the presence of Cu^{2+}), through the formation of a hydroxo complex. This dissociation pathway deteriorates the kinetic inertness of the complexes with small lanthanide ions, as demonstrated by the half-lives estimated at pH 7.4 ($[Cu^{2+}] = 1$ µM), which amount to 876 and 1.49×10^5 h for the Lu^{3+} and Gd^{3+} complexes, respectively. This prompted us to modify the design of H$_4$*CHX*OCTAPA to improve the kinetic properties of the complexes formed with small Ln^{3+} ions.

In this work, we report the synthesis of a new H$_4$*CHX*OCTAPA derivative, which we call H$_4$*CHX*OITAPA, in which the four arms attached to the cyclohexane-1,2-diamine unit are arranged so that the two picolinic acid groups are attached to the same amine N atom. This obviously changes the topology of the ligand with respect to the parent H$_4$*CHX*OCTAPA, as the donor atoms are arranged in a different manner. We hypothesized that the different topology of H$_4$*CHX*OCTAPA and H$_4$*CHX*OITAPA, along with other parameters, may affect the inertness of the complexes, as observed recently for the nonadentate chelators containing picolinate groups H$_4$NONEUNPA and H$_4$NONEUNPAX.[19,20] On the contrary, thermodynamic stability of Ln^{3+} complexes is primarily controlled by the number and nature of the donor atoms present in the ligand, with differences in stability of complexes with structurally related octa- and nonadentate ligands being often small.[21] In contrast to nonadentate H$_4$NONEUNPA and H$_4$NONEUNPAX, the ligands investigated here are octadentate. However, one should bear in mind that increasing ligand denticity does not necessarily enhance the thermodynamic stability and/or kinetic inertness of lanthanide complexes, as observed for some H$_4$DOTA derivatives.[22] As an example of acyclic ligands, octadentate $EGTA^{4-}$ forms Ln^{3+} complexes with lower stability and kinetic inertness than the analogues of heptadentate $OBETA^{4-}$ across most of the lanthanide series (Figure 1).[23,24] Thus, the thermodynamic stability of the Y^{3+} and Lu^{3+} complexes of H$_4$*CHX*OITAPA were determined and their dissociation kinetics investigated. The results are compared to those reported previously for the Lu^{3+} complex of H$_4$*CHX*OCTAPA. The structure of the complexes was investigated using a combination of NMR spectroscopy and DFT calculations. X-ray crystallography was applied for the [Y(H*CHX*OITAPA)(H$_2$O)] complex in order to gain direct structural information. Finally, to assess the potential of this chelator for radiopharmaceutical applications, radiolabeling experiments with the ^{90}Y- and ^{177}Lu-nuclides were also conducted.

2. Results and Discussion

2.1. Synthesis and X-Ray Structure

The syntheses of racemic H$_4$*CHX*OITAPA (Scheme 1) started from *trans*-*N*-Boc-1,2-cyclohexanediamine (**1**),[25] which was alkylated with ethyl 6-(chloromethyl)picolinate (**2**)[26] in acetonitrile using K_2CO_3 as a base, yielding intermediate **3** in 95% yield. Deprotection of **3** with trifluoroacetic acid in CH_2Cl_2 afforded compound **4** in 80% yield. Compound **4** was submitted to a second alkylation step with *tert*-butyl 2-bromoacetate in acetonitrile, followed by acid removal of the ethyl and *tert*-butyl ester groups, affording H$_4$*CHX*OITAPA in 37% yield over the two steps. This relatively low yield is likely related to the formation of lactams as byproducts due to the intramolecular reaction of the amine and ethyl

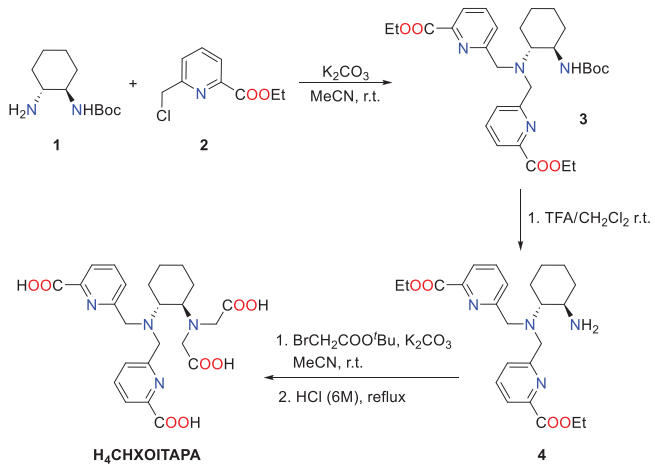

Scheme 1. Synthesis of H_4OITAPA.

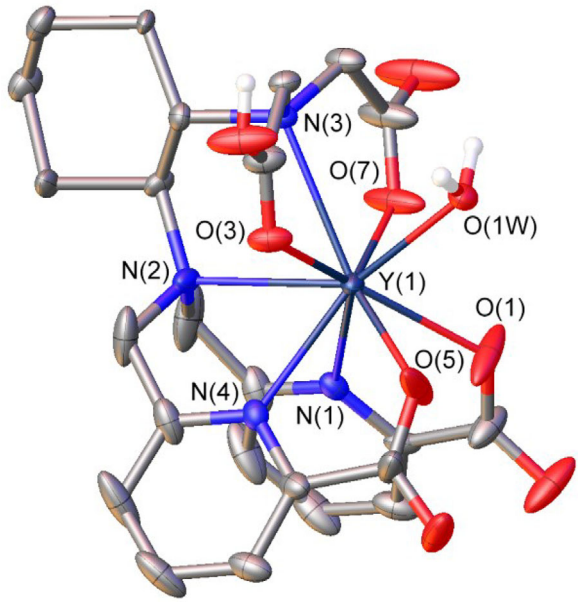

Figure 2. View of the X ray crystal structure of [Y(H*CHX*OITAPA)(H_2O)] with 30% ellipsoid probability. Hydrogen atoms attached to C atoms, water molecules, and the disorder of the cyclohexyl group were omitted for simplicity.

ester groups of **4**.[27] The complexes used for NMR were prepared by mixing stoichiometric amounts of the ligand and Y^{3+} or Lu^{3+} as their trifluoromethanesulfonate salts and subsequent adjustment of the pH with diluted NaOD solutions to reach a final concentration of ≈20 mM. Complex formation was confirmed by NMR and mass spectrometry (See Supporting Information for details).

Slow diffusion of acetone into an acidified aqueous solution of the Y^{3+} complex (pH ≈2) afforded single crystals suitable for X-ray diffraction measurements (Figure 2). Crystals contain the charge neutral [Y(H*CHX*OITAPA)(H_2O)] entity, in which one of the acetate groups is protonated, along with water molecules involved in hydrogen bond interactions with the carboxylate groups. The metal ion is nine-coordinated, being directly coordinated by the eight donor atoms of the ligand and a water molecule. The coordination polyhedron around the Y^{3+} ion can be best described as a capped square antiprism, in which the upper plane is defined by N(2)/O(3)/O(7)/O(1W) (rms deviation from planarity 0.113 Å) and the lower plane by N(1)/N(4)/O(1)/O(5) (rms deviation from planarity 0.020 Å), with the capping position being defined by N(3) (Figure 2). Shape measurements confirm the assignment of the coordination polyhedron with shape measures of 0.752 and 1.889 for a capped square antiprism and a tricapped trigonal prism, respectively (a shape measure of 0 indicates that the investigated polyhedron fully matches the reference polyhedron).[28] The two square planes define an angle of 6.2° and a torsion angle of 42.9 ± 4.3°, which are relatively close to the ideal values (0.0 and 45°, respectively).

Table 1. Bond distances of the Y^{3+} coordination environment in the X-ray structure of [Y(H*CHX*OITAPA)(H_2O)] ($d_{Y\text{-}D}$) compared with those estimated from donor radii and crystal radii (r_D + CR_Y) and the differences between them Δd [Å].

Donor type		$d_{Y\text{-}D}$	r_D + CR_Y	Δd[a]
carboxylate	Y(1)—O(1)	2.387(2)	2.346	0.041
	Y(1)—O(3)	2.391(2)	2.346	0.045
	Y(1)—O(5)	2.374(3)	2.346	0.028
	Y(1)—O(7)	2.262(2)	2.346	−0.084
amine	Y(1)—N(2)	2.659(2)	2.639	0.020
	Y(1)—N(3)	2.675(2)	2.639	0.036
Pyridine	Y(1)—N(1)	2.486(2)	2.543	−0.057
	Y(1)—N(4)	2.490(2)	2.543	−0.053
water	Y(1)—O(1W)	2.3389(19)	2.445	−0.106

[a] $\Delta d = d_{Y\text{-}D} - (r_D + CR_Y)$, and thus negative values indicate that the observed distances ($d_{Y\text{-}D}$) are shorter than the reference values (r_D + CR_Y).

The number of X-ray structures reported for Y^{3+} complexes with polyaminopolycarboxylate (PAC) ligands is scarce,[29–33] with very few structures containing picolinate groups.[34] Furthermore, a significant number of the structures display eight-coordinated Y^{3+} ions,[35,36] and thus the bond distances of the metal coordination environment cannot be directly compared with those of [Y(H*CHX*OITAPA)(H_2O)]. Thus, we sought to analyze the data reported here by comparing the observed distances ($d_{Y\text{-}D}$) with those estimated by the sum of the crystal radius of Y^{3+} (CR_Y) for coordination number nine (1.214 Å)[37,38] and the donor radii (r_d) estimated recently from the analysis of a large number of structures of rare-earth complexes (Table 1).[39] The differences between the experimental and reference values (Δd) evidence that the distances involving amine N atoms [Y(H*CHX*OITAPA)(H_2O)] are only slightly longer than those predicted from donor radii, while those to pyridine N atoms are ≈0.05 Å shorter. Concerning the carboxylate donor atoms, three of them give distances that are longer than the reference value of 2.346 Å, while the Y(1)—O(7) distance is up to 0.084 Å shorter than r_D + CR_Y, indicating that the latter carboxylate group provides a particularly strong interaction with the metal ion. Nevertheless, the average Y—O distance involving carboxylate groups (2.353 Å) is very close to the reference value estimated from donor radii. Finally, the Δd value obtained for

Y(1)—O1 W evidences a rather strong binding of the coordinated water molecule. This may be attributed to the coordination of the water molecule on one of the square faces of the square antiprismatic coordination polyhedron, rather than at a capping position.

2.2. NMR Spectra

The ^{1}H and ^{13}C NMR spectra of the Y^{3+} and Lu^{3+} complexes of *CHX*OITAPA^{4-} are well resolved and display the 24 resonances expected for a single species with a C_1 symmetry in solution. The ^{1}H spectra are characteristic of rigid species with well-defined AB spin systems for the methylenic protons (Figure S9). The very similar spectra obtained for the two complexes indicate that they have comparable structures in solution. A full assignment of the spectra was achieved with the aid of 2D ^{1}H-^{1}H COSY and ^{1}H-^{13}C HSQC and HMBC experiments (Tables S1 and S2). For comparative purposes, we also recorded the ^{1}H and ^{13}C NMR spectra of [Y(*CHX*OCTAPA)]$^{-}$, which were not reported previously.

One of the signals due to the pyridyl protons is considerably more shielded in the spectra of *CHX*OITAPA^{4-} (δ = 7.18 and 7.11 ppm for the Y^{3+} and Lu^{3+} complexes, respectively) than in the corresponding *CHX*OCTAPA^{4-} complexes (δ = 7.62 and 7.55 ppm for the Y^{3+} and Lu^{3+} complexes, respectively). Another significant difference that becomes evident when comparing the ^{1}H NMR spectra of *CHX*OCTAPA^{4-} and *CHX*OITAPA^{4-} complexes concerns the chemical shifts of the resonances of the C-H protons of the cyclohexyl ring at a two-bond distance from the amine N atoms. These protons display very similar chemical shifts in [Y(*CHX*OITAPA)]$^{-}$ (δ = 3.03 and 3.09 ppm), but they differ by up to 1.12 ppm in [Y(*CHX*OCTAPA)]$^{-}$ (δ = 3.01 and 1.89 ppm). In the latter case, the proton at δ = 1.89 ppm is shielded by the ring current of one of the picolinate groups, as demonstrated from the analysis of the paramagnetic ^{1}H shifts observed for the Yb^{3+} analogue.[3] This situation is not observed in [Y(*CHX*OITAPA)]$^{-}$, where the two picolinate groups are folded in opposite direction with respect to the cyclohexyl group (see Figure 2). Thus, the NMR spectra of [Y(*CHX*OITAPA)]$^{-}$ are consistent with the structure observed in the solid state.

Further information on the structure of [Y(*CHX*OITAPA)]$^{-}$ was gained by analyzing the ^{1}H—^{89}Y HMQC NMR spectrum, which shows cross-peaks relating the ^{89}Y nucleus and several methylenic protons of the acetate and picolinate arms (Figure 3). The observed ^{89}Y chemical shift (δ = 89.9 ppm) is very similar to those determined for [Y(*CHX*OCTAPA)]$^{-}$ and [Y(OCTAPA)]$^{-}$, indicating that the Y^{3+} ions in these complexes are coordinated by identical donor atom sets (Table 2). Indeed, the ^{89}Y chemical shift was found to be very sensitive to the number and type of donor atoms coordinated to the metal ion, but rather insensitive to their arrangement in the metal coordination sphere.[34,36] Furthermore, an empirical relationship proposed to estimate ^{89}Y chemical shift shifts provides δ = 72 ppm for these complexes, when considering a donor set comprised by 2 amine N atoms, two pyridyl N atoms, four carboxylate O atoms, and an O atom of a water molecule.[36] The ^{89}Y NMR signal of [Y(*CHX*OITAPA)]$^{-}$ is shifted to lower fields in comparison with [Y(*CHX*OCTAPA)]$^{-}$ and [Y(OCTAPA)]$^{-}$, but the magnitude of this shift (< 15 ppm, Table 2) is small compared with the shielding contributions of different donor atoms (> 70 ppm) and the chemical shift range observed for Y^{3+} complexes in aqueous solution, which spans ≈270 ppm. [36] These results confirm that this family of ligands forms nine-coordinate complexes in aqueous solution through binding of the octadentate ligand and coordination of a water molecule. The ^{89}Y chemical shifts were also estimated with scalar relativistic DFT calculations at the TPSSh/ZORA/Def2-TZVPP level (see computational methods below for details). For this purpose, the structure of [Y(*CHX*OITAPA)]$^{-}$ was optimized starting from the X-ray structure, after incorporating two explicit second-sphere water molecules involved in hydrogen bonds with the coordinated water molecule. For [Y(OCTAPA)]$^{-}$ and [Y(*CHX*OCTAPA)]$^{-}$ similar structures were obtained using input structures reported in our previous works (Figure S30).[3,5] These calculations yield ^{89}Y chemical shifts in excellent agreement with the experimental values, indicating that these DFT models provide an excellent description of the structure of the complexes in solution. The three complexes of the OCTAPA^{4-} family display

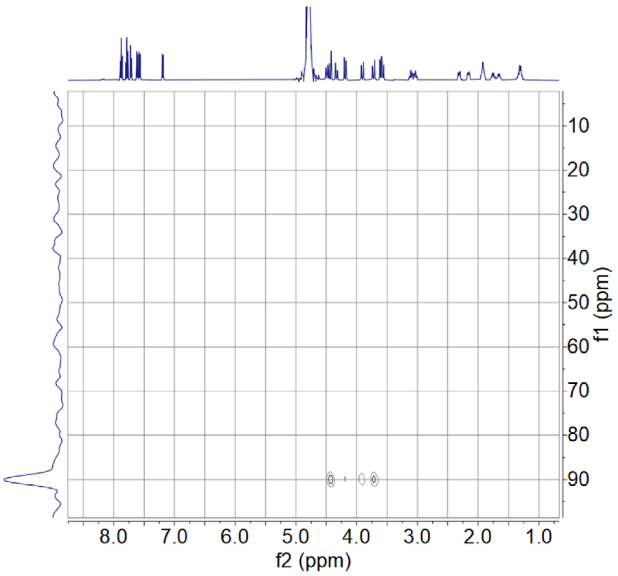

Figure 3. ^{1}H,^{89}Y-HMQC NMR spectrum of [Y(H*CHX*OITAPA)(H_2O)] recorded in D_2O solution (500 MHz, pH = 6.84, 298 K).

Table 2. Experimental (δ_{exp}) and calculated (δ_{calc}) ^{89}Y NMR shifts (ppm), isotropic shielding constants (σ_{iso}) and diamagnetic (σ_d) and paramagnetic (σ_p) contributions. All data in ppm.[a]

	σ_{iso}	σ_d	σ_p	δ_{calc}	δ_{exp}
[Y(OCTAPA)(H_2O)]$^{-}$	2673.4	3744.0	−1070.6	76.2	75.6
[Y(*CHX*OCTAPA)(H_2O)]$^{-}$	2672.0	3746.7	−1074.7	77.6	77.8
[Y(*CHX*OITAPA)(H_2O)]$^{-}$	2668.4	3746.0	−1077.5	81.2	89.9
$[Y(H_2O)_8]^{3+}$·16H_2O[b]	2749.6	3771.7	−1022.1	0	0

[a] Isotropic shielding constants and their contributions calculated at the TPSSh/ZORA/Def2-TZVPP level.
[b] Data from Ref. [41]

Table 3. Stability constants of the Y^{3+}, Gd^{3+} and Lu^{3+} complexes and protonation constants of the complexes and the chelators (I = 0.15 M NaCl, 25 °C).

	*CHX*OITAPA^{4-}	*CHX*OCTAPA^{4-}	OCTAPA^{4-}
log K_1^H	11.32(1)	9.52[a] / 9.23[b]	8.52[c] / 8.58[d]
log K_2^H	5.46(2)	5.51[a] / 5.40[b]	5.40[c] / 5.43[d]
log K_3^H	4.28(2)	3.99[a] / 3.94[b]	3.65[c] / 3.75[d]
log K_4^H	2.75(3)	3.43[a] / 2.24[b]	2.97[c] / 3.08[d]
log K_5^H	1.84(2)	1.59[a] / 1.82[b]	1.66[c] / 2.21[d]
Σlog K_i^H (i = 1–5)	25.65	24.03[a]	22.20[c] / 23.05[d]
log K_{GdL}	21.47(4)	19.92[a]	20.23[c]
pGd	22.43	20.87	21.18
log K_{YL}	21.24(5)	19.19[a]	18.30[e]
pY	22.19	20.14	19.25
log K_{LuL}	21.96(1)	–	20.49[c] / 20.08[e]
pLu	22.91	–	21.44

[a] Data from Ref. [3]
[b] Data from Ref. [8]
[c] Data from Ref. [5]
[d] Data from Ref. [6] in 0.16 M NaCl; Values of log K_6^H = 0.12 and log K_7^H = -0.46 were also reported.
[e] Data from Ref. [42]

very similar diamagnetic and paramagnetic contributions to the ^{89}Y chemical shifts (Table 2).[40]

2.3. Protonation Constants and Thermodynamic Stability Constants

The protonation constants of *CHX*OITAPA^{4-} were determined using 0.15 M NaCl as background electrolyte. The logK_i^H values obtained from the fits of the titration curves are compared with those reported previously for OCTAPA^{4-} and *CHX*OCTAPA^{4-} in Table 3. The value of logK_1^H determined for *CHX*OITAPA^{4-} is ≈2 log units higher than that reported for *CHX*OCTAPA^{4-}. This is the result of the electron withdrawing effect of the picolinate group described previously,[2] which decreases the basicity of both amine N atoms of *CHX*OCTAPA^{4-}. Thus, the first protonation constant in *CHX*OITAPA^{4-} takes place on the amine N atom of the ligand functionalized with two carboxylate groups. The electron withdrawing effect of the picolinate group becomes evident when comparing the logK_1^H values reported for MIDA^{2-} (H_2MIDA = 2,2′-(methylazanediyl)diacetic acid; logK_1^H = 9.43–9.65 at 25 °C)[43] and DPAMA^{2-} (H_2DPAMA = 6-(((6-carboxypyridin-2-yl)(methyl)amino)methyl)picolinic acid, logK_1^H = 7.82 at 25 °C in 0.15 M NaCl).[44]

The second protonation constant, characterized by logK_2^H, corresponds to the protonation of the second amine N atom, and takes similar values for the three ligands. Subsequent protonation constants are associated with carboxylate groups. The *CHX*OITAPA^{4-} and *CHX*OCTAPA^{4-} ligands are characterized by similar overall basicities, as evidenced by the values of Σlog K_i^H (i = 1–5, Table 3). The basicity of the cyclohexyl derivatives is higher than that of OCTAPA^{4-}, an effect related to the electron-donating effect of the cyclohexyl ring.[45]

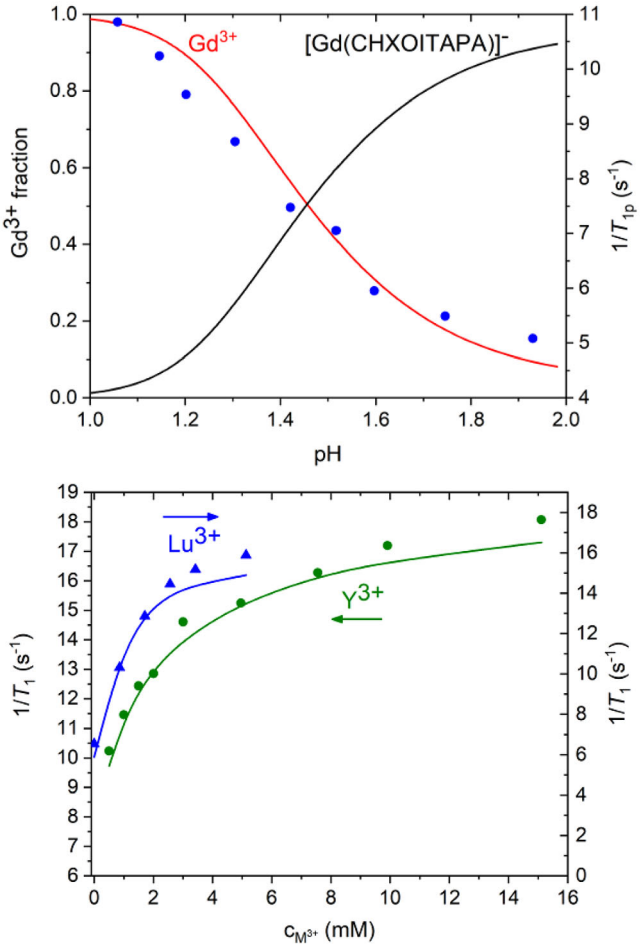

Figure 4. Top: Variation of the longitudinal relaxation rate ($1/T_1$, 60 MHz, 25 °C) with pH of a solution containing 1.50 mM Gd^{3+} and 1.43 mM *CHX*OITAPA^{4-} and the distribution curves calculated from thermodynamic data. Bottom: Variation of the longitudinal relaxation rate ($1/T_1$, 20 MHz, 25 °C) for solutions of [Gd(*CHX*OITAPA)]$^{4-}$ upon addition of Lu^{3+} ([Gd^{3+}] = 1.3 mM, pH 4.57, 0.05 M DMP buffer) or Y^{3+} ([Gd^{3+}] = 1.5 mM, pH 4.59, 0.05 M DMP buffer).

As discussed in our previous work,[5] lanthanide complexes with OCTAPA^{4-} derivatives dissociate at rather low pH (< ≈2), and thus direct potentiometry alone is unsuitable for stability constant determination. Thus, potentiometric data must be supported by another technique. Herein, we first determined the stability constant of the Gd^{3+} ion using the relaxometric method, which consists in measuring the relaxation rate of the ^1H NMR water signal of the solution in the pH range where complex dissociation takes place. We measured both longitudinal ($1/T_1$) and transverse ($1/T_2$) relaxation rates at two different magnetic fields corresponding to proton Larmor frequencies of 20 and 60 MHz. The relaxation rates measured for an equimolar solution of Gd^{3+} and *CHX*OITAPA^{4-} increase below pH 2 as a result of complex dissociation, due to the formation of the $[Gd(H_2O)_8]^{3+}$ species (Figure 4).[46] The simultaneous fit of the four sets of relaxometric data afforded a stability constant of log K_{GdL} = 21.47(4). Subsequently, the stability constants of the Y^{3+} and Lu^{3+} analogues were obtained by relaxometric titration of the Gd^{3+} complex with the corresponding diamagnetic ion (Figure 4). This allowed

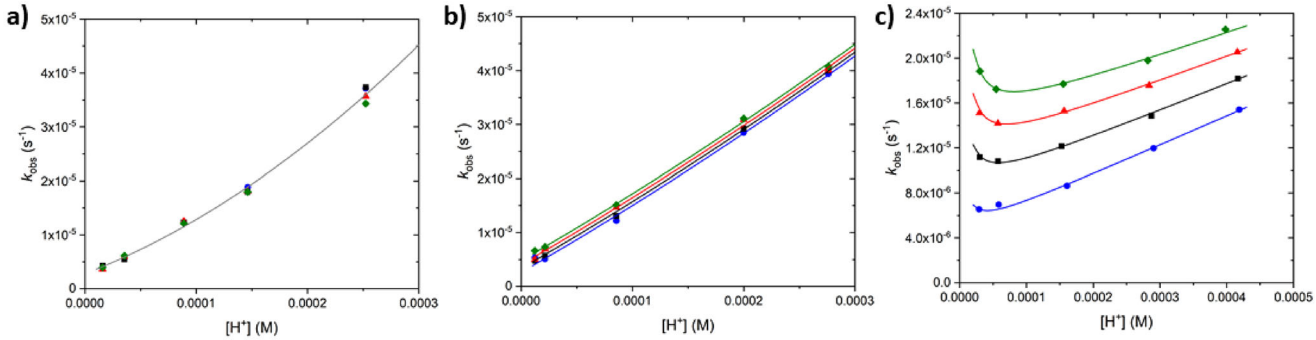

Figure 5. Plot of the pseudo-first-order rate constants measured for the dissociation of the complexes as a function of H^+ ion concentration (50 mM DMP, 25 °C, 0.15 M NaCl) using different metal ion excess; a) [Lu(*CHX*OITAPA)]$^-$ [10× (3.02 mM), 20× (6.04 mM), 30× (9.06 mM), and 40×(12.08 mM) at pH = 3.66, 3.89, 4.05, 4.43, and 4.76]; b) [Y(*CHX*OITAPA)]$^-$ [10× (3.95 mM), 20× (7.90 mM), 30× (11.8 mM), and 40×(17.78 mM) at pH = 3.56, 3.70, 4.07, 4.67, and 4.91]; c) [Y(*CHX*OCTAPA)]$^-$ [10× (5.53 mM), 20× (11.07 mM), 30× (16.60 mM), and 40×(22.14 mM) at pH = 3.30, 3.50, 3.80, 4.17, and 4.49].

us to obtain the stability constants for the Ln^{3+} (Ln^{3+} = Y^{3+} or Lu^{3+}) complexes following the exchange reactions (Eq. (1)).

$$[Gd(CHXOITAPA)]^- + Ln^{3+} \leftrightarrows [Ln(CHXOITAPA)]^- + Gd^{3+} \quad (1)$$

The stability constants shown in Table 2 indicate that the *CHX*OITAPA^{4-} complexes are significantly more stable than the corresponding *CHX*OCTAPA^{4-} analogues, in spite of the very similar basicities of the two ligands. This highlights the impact that a different ligand topology may have on the stability of the complexes. The complexes of OCTAPA^{4-} also show lower stabilities than the *CHX*OITAPA^{4-} analogues. The high log K_{LnL} values of the *CHX*OITAPA^{4-} complexes are translated to the corresponding pM values, defined as the -log[M]$_{free}$ at pH 7.4 for a metal concentration of 1 μM and a ligand concentration of 10 μM.[47] The pM values obtained from equilibrium data for the *CHX*OITAPA^{4-} complexes are consistently higher than those of the corresponding *CHX*OCTAPA^{4-} and OCTAPA^{4-} complexes, indicating a higher thermodynamic stability of the *CHX*OITAPA^{4-} complexes at physiological pH. It is also worth noting that the stability constant determined for the Lu^{3+} complex of octadentate *CHX*OITAPA^{4-} (log K_{LuL} = 21.96) is very similar to those reported for nonadentate H_4NONEUNPA (log K_{LuL} = 21.49)[19,20] and H_4NONEUNPAX (log K_{LuL} = 21.93), showing that the increased ligand denticity does not translate into a higher thermodynamic stability for this series of structurally related chelators.

2.4. Dissociation Kinetics

The inertness of a metal complex with respect to dissociation is believed to be more important for pharmaceutical applications than thermodynamic stability. Thus, we conducted a detailed study of the dissociation kinetics of the *CHX*OITAPA^{4-} complexes with Y^{3+} and Lu^{3+} by following the exchange reactions with Cu^{2+}, which was used in large excess (10-40 equivalents) to ensure pseudo-first-order conditions. The exchange reactions were conducted in the approximate pH range 3.4 –4.8. For the sake of comparison, we also investigated the dissociation of [Y(*CHX*OCTAPA)]$^-$, which was not reported previously, in the pH range 3.3–4.5 (Figure 5). The reactions were followed by UV absorption spectroscopy following the absorption of the Cu^{2+} complexes at 310 nm.

The rates of dissociation (k_{obs}) of the [Lu(*CHX*OITAPA)]$^-$ complex increase with proton concentration, indicating that the proton-assisted mechanism assists complex dissociation (Figure 5). The trend observed in the plot of k_{obs} versus [H^+] evidences a quadratic dependence of the dissociation rate with proton concentration. The experiments performed using different Cu^{2+} concentrations yield the same values of k_{obs} within experimental error, indicating that the metal-assisted pathway does not contribute significantly under the conditions used. The Y^{3+} analogue shows a similar behavior, although a slight dependence of the dissociation rates with Cu^{2+} concentration is observed, indicating that the metal-assisted pathway contributes significantly to complex dissociation.

The behavior observed for the *CHX*OITAPA^{4-} is in sharp contrast to that of the Y^{3+} complex of *CHX*OCTAPA^{4-}. The latter complex shows a linear increase of the dissociation rates with proton concentration for [H^+] > 10^{-4} M, with no quadratic dependence being observed. At low proton concentrations, the values of k_{obs} increase, which evidences the presence of a base-catalyzed mechanism due to the formation of a hydroxo heterodinuclear species Y(L)Cu(OH), as observed previously for the Lu^{3+} analogue.[3] The different dissociation pathways observed for the complexes investigated in this work are summarized in Scheme 2. Taking into account these pathways, the dependence of the dissociation rate constants (k_{obs}) with proton and Cu^{2+} concentration can be expressed as shown in Scheme 2.[3,5] The values of K_{CuOH} ($10^{-7.98}$)[48] and K_w ($10^{-13.77}$ at 25 °C and 0.15 M NaCl)[49,50] were fixed during the analysis.

The results of the least-squares fit of the kinetic data are shown in Table 4. The complexes of *CHX*OITAPA^{4-} display a significant contribution of the spontaneous dissociation, characterized by k_0, which is given by the intercept of k_{obs} with the *y* axis at [H^+] = 0. This is in contrast with the *CHX*OCTAPA^{4-} complexes, which do not show significant dissociation through the spontaneous mechanisms under the conditions used for the kinetic experiments. The fit of the data confirms that the acid-catalyzed dissociation in *CHX*OITAPA^{4-} complexes proceeds through the formation of mono- and di-protonated species, characterized by k_1 and k_2, respectively. The value of k_2 is higher

Table 4. Rate and equilibrium constants characterizing the dissociation of the Y^{3+} and Lu^{3+} complexes of *CHX*OITAPA^{4-} and *CHX*OCTAPA^{4-} (I = 0.15 M NaCl, 25 °C).

	*CHX*OITAPA^{4-}		*CHX*OCTAPA^{4-}	
	Y^{3+}	Lu^{3+}	Y^{3+}	Lu^{3+}[a]
k_0 [s^{-1}]	(2.4 ± 0.4)×10^{-6}	(2.7 ± 0.4)×10^{-6}	—	—
k_1 [M^{-1} s^{-1}]	0.106 ± 0.010	0.080 ± 0.009	0.0286 ± 0.0004	0.0374
k_2 [M^{-2} s^{-1}]	99 ± 44	203 ± 31	—	—
k_3^{Cu} [M^{-1} s^{-1}]	(1.5 ± 0.3)×10^{-4}	—	(8.5 ± 0.2)×10^{-4}	6.3×10^{-4}
k_6^{Cu} [M^{-2} s^{-1}]	—	—	(4.9 ± 0.2)×10^{5}	5.1×10^{5}
K_{Cu}	—	—	17 ± 1	12.1
$t_{1/2}$ [h][b]	102	69	910	876

[a] Data from Ref. [3]
[b] Calculated from the rate constants as (ln2)/k_{obs} at pH 7.4 for [Cu^{2+}] = 1 μM.

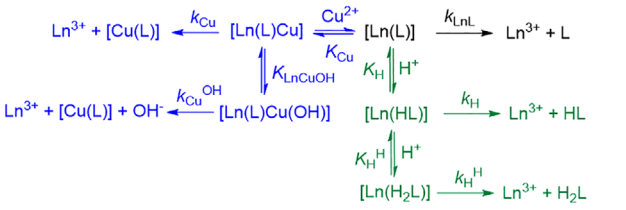

$$k_{obs} = \frac{k_0 + k_1[H^+] + k_2[H^+]^2 + k_3^{Cu}[Cu^{2+}] + k_6^{Cu}[Cu^{2+}]K_w/[H^+]}{1 + K_H[H^+] + K_H^H[H^+]^2 + K_{Cu}[Cu^{2+}] + K_{CuOH}K_{Cu}[Cu^{2+}]K_w/[H^+]}$$

$$k_0 = k_{LnL},\ k_1 = k_H K_H,\ k_2 = k_H^H K_H K_H^H,\ k_3^{Cu} = k_{Cu}K_{Cu},\ k_6^{Cu} = k_{Cu}^{OH}K_{Cu(OH)}$$

$$K_H = \frac{[Ln(HL)]}{[Ln(L)][H^+]};\quad K_H^H = \frac{[Ln(H_2L)]}{[Ln(HL)][H^+]}\quad K_{Cu} = \frac{[Ln(L)Cu]}{[Ln(L)][Cu^{2+}]};$$

$$K_{CuOH} = \frac{[Cu(OH)^+]}{[OH^-][Cu^{2+}]};\qquad K_w = [OH^-][H^+];$$

Scheme 2. Dissociation pathways of the Y^{3+} and Lu^{3+} complexes investigated in this work: spontaneous (black), proton-assisted (green), and metal-assisted (blue), and expressions used to analyze the kinetic data.

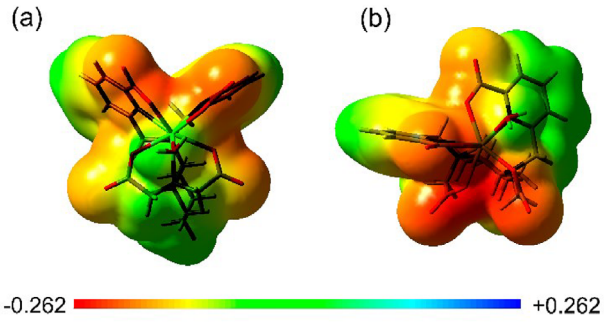

Figure 6. Electrostatic potential (a. u.) mapped on isoelectronic surfaces of 0.001 a. u. for [Y(*CHX*OITAPA)(H_2O)]$^-$ a) and [Y(*CHX*OCTAPA)(H_2O)]$^-$ b).

for the Lu^{3+} complex than for the Y^{3+} one, as expected from the more evident quadratic dependence of k_{obs} in the former (Figure 5). Of note, the protonation constants K_H and K_H^H are low enough so that the $K_H[H^+]$ and $K_H[H^+]^2$ products are $<<1$, and thus cannot be determined from the kinetic data. The values of k_1 are significantly higher for the *CHX*OITAPA^{4-} complexes compared with the *CHX*OCTAPA^{4-} analogues, indicating the former are more prone to dissociation following the acid-dissociation mechanism. The opposite situation occurs for the Cu^{2+}-catalyzed mechanisms, which contribute significantly to the dissociation of the *CHX*OCTAPA^{4-} complexes close to neutral pH, but it is negligible for the complexes of *CHX*OITAPA^{4-}. These results evidence that the different topologies of these ligands affect very significantly the dissociation pathways leading to complex dissociation. The half-lives calculated from rate constants at pH 7.4 for a Cu^{2+} concentration of 1 μM (Table 4) evidence that the *CHX*OITAPA^{4-} complexes are more labile than the *CHX*OCTAPA^{4-} analogues, which is mainly the result of a faster acid-catalyzed dissociation for the former chelate.

The analysis of the DFT structures calculated for the Y^{3+} complexes provides some hints on the dissociation mechanisms observed for the complexes of *CHX*OCTAPA^{4-} and *CHX*OITAPA^{4-}. The [Y(*CHX*OITAPA)(H_2O)]$^-$ complex displays a rather long Y—O distance involving an oxygen atom of an acetate group (2.397 Å) when compared with [Y(*CHX*OCTAPA)(H_2O)]$^-$ (2.300 and 2.328 Å, Table S7). The acid-catalyzed dissociation mechanism requires the protonation of the complex, very likely at a carboxylate group being weakly bound to the metal ion (as evidenced during the X-ray crystallograpic studies). Subsequent carboxylate de-coordination and transfer of the proton to an amine N atom triggers complex dissociation. A weak interaction of a carboxylate group is expected to favor this process, making proton-assisted dissociation more favorable. On the other hand, the Cu^{2+}-assisted process involves the formation of a dinuclear intermediate [Ln(L)Cu)] (Scheme 2). The electrostatic potential calculated for the [Y(*CHX*OITAPA)(H_2O)]$^-$ (a) and [Y(*CHX*OCTAPA)(H_2O)]$^-$ (b) complexes on isosurfaces defined by electron densities of 0.001 a. u.[51] are shown in Figure 6. The most negative electrostatic potentials are computed on the regions where the carboxylate donor groups are situated, as would be expected. However, one can notice significant differences for the two complexes, with [Y(*CHX*OCTAPA)(H_2O)]$^-$ being characterized by a more negative electrostatic potential (red color in Figure 6). This is very likely facilitating the formation of the dinuclear [Ln(L)Cu)] complex, thus favoring the metal-assisted pathway.

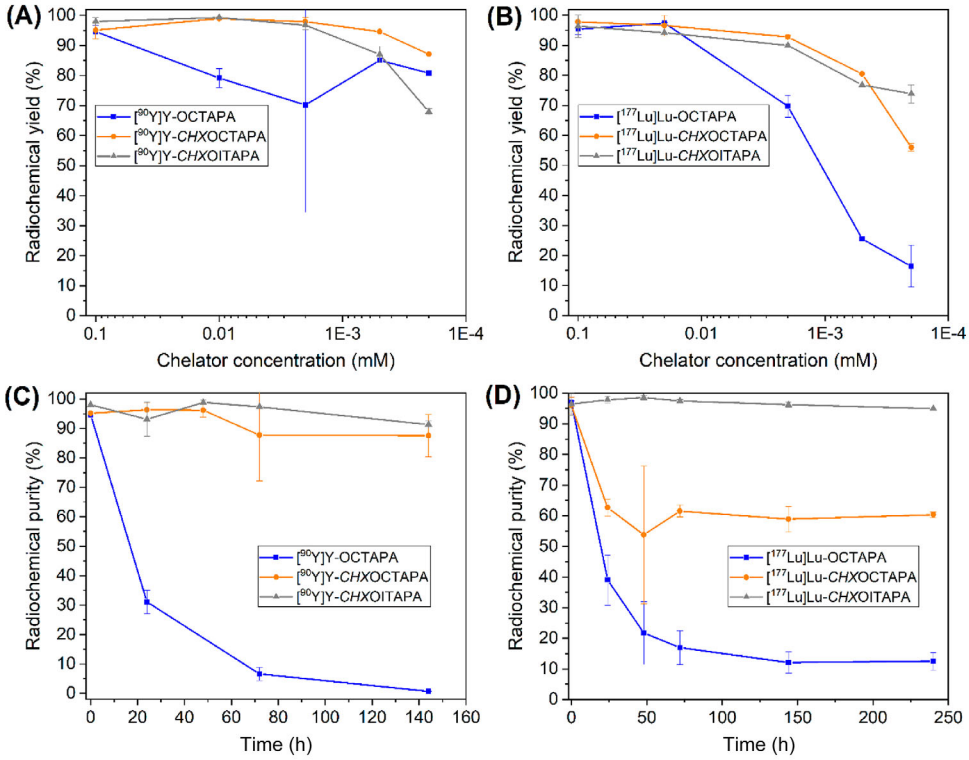

Figure 7. A) and B): Concentration-dependent radiolabeling of H_4*CHX*OITAPA, H_4*CHX*OCTAPA, and H_4OCTAPA with $^{90}Y^{3+}$ (10–50 MBq) (A) and $^{177}Lu^{3+}$ (20–40 MBq) (B), after 5 min reaction time at room temperature in NH_4OAc (10 mM, pH 5.5). C) and D): Stability (% intact complex remaining) measured at various time points after incubating the [^{90}Y]Y- (C) and [^{177}Lu]Lu (D) complexes of *CHX*OITAPA^{4-}, *CHX*OCTAPA^{4-}, and OCTAPA^{4-} in human serum at 37 °C.

2.5. Radiolabeling

Remarkably, quantitative radiolabeling of *CHX*OITAPA^{4-} was achieved with ^{90}Y and ^{177}Lu in just 10 min at chelator concentrations as low as 2×10^{-6} M. Representative high-performance liquid chromatography (HPLC) chromatograms of the different radio-complexes are given in Figures S26 and S27. Heating and longer reaction times were thus not investigated. The results obtained with *CHX*OITAPA^{4-} compare favorably with OCTAPA^{4-} (Figure 7). Surprisingly, while *CHX*OITAPA^{4-} appeared to be able to chelate ^{177}Lu with higher radiochemical yield (RCY) than *CHX*OCTAPA^{4-} at lower ligand concentration, it is the opposite with ^{90}Y. With the final ligand concentration of 2×10^{-7} M, RCY was 67.91 ± 0.96% for [^{90}Y]Y(*CHX*OITAPA)$^-$ and 73.85 ± 3.04% for [^{177}Lu]Lu(*CHX*OITAPA)$^-$, while it was respectively 87.10 ± 0.12% for [^{90}Y]Y(*CHX*OCTAPA)$^-$ and 56.00 ± 1.27% for [^{177}Lu]Lu(*CHX*OCTAPA)$^-$. The influence of the pH was also investigated, using various acetate buffers. Over a pH range of 4.5–7.0, there was no significant change in the RCYs obtained, whatever the ligand and the radiometal, except for H_4OCTAPA, with a lower RCY, slightly below 90% at the highest pH investigated (85.60 ± 10.89% at pH = 7.0, Figures S28 and S29).

To evaluate and compare the stability of these ligands in biologically relevant media, they were radiolabeled with ^{90}Y and ^{177}Lu and incubated in human blood serum as a transchelation challenge. The amount of radiometal transchelated from ligands to serum proteins was assessed at different time points by radio-thin-layer chromatography (radio-TLC) after protein denaturation. The results represented in Figure 7 reveal that the rigidified versions of H_4OCTAPA demonstrated a higher stability in human serum during a 6-day period with ^{90}Y. The same is true with ^{177}Lu over 10 days, though [^{177}Lu]Lu(*CHX*OCTAPA)$^-$ appeared to be less stable than its ^{90}Y analogue. The latter complex shows an unusual behavior, as only a fraction of the radiolabeled complex appears to dissociate in serum. The radio-HPLC trace of the complex indeed shows that two complex species of *CHX*OCTAPA^{4-} are formed with relative abundances of 59:41. This situation is also observed for the [^{90}Y]Y^{3+} analogue, although the relative abundance of the two forms is slightly different (66:34). This is in sharp contrast with the radio-HPLC traces of the *CHX*OITAPA^{4-} and OCTAPA^{4-}, which evidence the formation of a single complex species. The two complex species observed for the radio-complexes of *CHX*OCTAPA^{4-} are very likely the (*S*,*R*) and (*S*,*S*) isomers described in our previous work.[3]

The H_4*CHX*OITAPA chelator appears particularly suited for labeling with ^{90}Y and ^{177}Lu, as it provides the highest stability in serum among the three chelators investigated here and appears to form a single isomer, in contrast to H_4*CHX*OCTAPA. Thus, H_4*CHX*OITAPA is the most promising candidate of the OCTAPA family investigated so far for the development of ^{90}Y- and ^{177}Lu-based radiopharmaceuticals. It is thus interesting to investigate these ligands coupled to a biomolecule, since results sometimes diverge between the biomolecule-coupled radiocomplex and its non-bifunctional version.[52]

3. Conclusion

In this work, we have expanded the family of OCTAPA^{4-} chelators by preparing and characterizing H$_4$*CHX*OITAPA. This chelator preserves the rigid cyclohexyl spacer that was found previously to be crucial on enhancing the kinetic inertness of rare-earth complexes, but changes the topology of the ligand by attaching the two picolinate groups to the same amine N atom. This structural modification is beneficial in terms of complex stability, as both the Y^{3+} and Lu^{3+} complexes of *CHX*OITAPA^{4-} are more stable than the *CHX*OCTAPA^{4-} and OCTAPA^{4-} analogues. Both cyclohexyl derivatives form Y^{3+} and Lu^{3+} complexes that are remarkably more inert than those formed by the parent OCTAPA^{4-}, as a result of the rigidifying effect of the cyclohexyl fragment. Dissociation kinetic studies indicate that the complexes of H$_4$*CHX*OITAPA dissociate following the spontaneous and acid-catalyzed dissociation pathways, with the Cu^{2+}-promoted mechanisms providing a slight contribution in the case of the Y^{3+} complex. This is in contrast with the complexes of H$_4$*CHX*OCTAPA, for which the Cu^{2+}-assisted mechanism represents the main dissociation pathway at pH 7.4. These results highlight that ligand topology can affect significantly the dissociation pathways of rare-earth complexes of OCTAPA derivatives.

The three OCTAPA derivatives studied here can be quantitatively radiolabeled with ^{90}Y and ^{177}Lu in just 10 min at room temperature. The presence of the cyclohexyl unit enhances considerably the stability of the radio-complexes in human serum, with both *CHX*OITAPA^{4-} and *CHX*OCTAPA^{4-} performing significantly better than OCTAPA^{4-}. Finally, *CHX*OITAPA^{4-} is better suited than *CHX*OCTAPA^{4-} for stable [^{177}Lu]Lu^{3+} chelation, as in the latter case partial dissociation is observed in human serum at 37 °C. Thus, *CHX*OITAPA^{4-} appears to be the most promising OCTAPA derivative for the development of ^{177}Lu-based radiopharmaceuticals.

4. Experimental Section

General Considerations: The H$_4$*CHX*OCTAPA and H$_4$OCTAPA ligands were prepared as described previously in the literature.[5,7] All other chemicals and solvents were purchased from commercial sources and used without further purification. The complexes used for NMR were prepared by mixing stoichiometric amounts of the ligand and the metal trifluoromethanesulfonate salts, Y(OTf)$_3$ or Lu(OTf)$_3$, and subsequent adjustment of the pH with diluted NaOD solutions to give a final concentration of ≈20 mM.

Medium Performance Liquid Chromatography (MPLC) was carried out using a Puriflash XS 420 InterChim Chromatographer equipped with a UV-DAD detector and a 20 g BGB Aquarius C18AQ reversed-phase column (100 Å, spherical, 15 µm), using a mixture of H$_2$O and CH$_3$CN with 0.1% TFA as the mobile phase. High resolution Mass Spectra (ESI-TOF) were recorded in the positive mode using a LTQ-Orbitrap Discovery Mass Spectrometer.^{1}H and ^{13}C NMR spectra were recorded using Bruker AVANCE III 300, Bruker AVANCE 400 or Bruker AVANCE 500 spectrometers. ^{89}Y NMR spectra were recorded on a Bruker AVANCE 400 spectrometer.

Synthesis of the chelator: **Diethyl 6,6′-(((*trans*-2-((tert-butoxycarbonyl)amino) cyclohexyl)azanediyl)bis(methylene))dipicolinate (3)** A solution of ethyl 6-(chloromethyl)picolinate[26] (**2**, 0.4672 g, 2.340 mmol) in CH$_3$CN (10 mL) was added dropwise to a solution of *trans*-*N*-Boc-1,2-cyclohexanediamine[25] (**1**, 0.2508 g, 1.170 mmol) containing K$_2$CO$_3$ (0.4043 g, 2.926 mmol) in CH$_3$CN (35 mL). A catalytic amount of KI was added, and the mixture was purged with an argon flow while stirred at room temperature for 7 days. The reaction mixture was filtered, and the filtrate was evaporated to dryness in vacuo, giving a yellow solid (0.5996 g, 95%). The crude product was used in the next step without further purification. ^{1}H-NMR (500 MHz, Chloroform-d) δ 7.93 (d, J = 7.7 Hz, 2H), 7.65 (m, 2H), 7.52 (d, J = 8.0 Hz, 2H), 4.48 (m, 4H), 3.96 (s, 4H), 3.54 (s, 1H), 2.64 (t, J = 10.9 Hz, 1H), 2.23 (d, J = 13.7 Hz, 1H), 2.11 (m, 1H), 1.81 (d, J = 13.1 Hz, 1H), 1.67 (d, J = 13.2 Hz, 1H), 1.27 (m, 20H).^{13}C-NMR (126 MHz, Chloroform-d) δ 165.76, 161.53, 156.37, 147.92, 137.41, 126.35, 123.66, 62.23, 55.64, 34.63, 28.97, 25.80, 25.27, 14.66, 2.28. MS (ESI$^+$, MeOH/H$_2$O): *m/z* 541.3016; calculated for [C$_{29}$H$_{41}$N$_4$O$_6$]$^+$ 541.3021.

Diethyl 6,6′-(((*trans*-2-aminocyclohexyl)azanediyl) bis(methylene))dipicolinate (4). Compound **3** (352.5 mg, 0.65 mmol) was dissolved in dichloromethane (7 mL), and trifluoracetic acid (7 mL) was added. The orange mixture was left stirring overnight at room temperature. After this time, the mixture was evaporated under vacuum. The solid residue was treated with 20 mL of an aqueous solution of KOH and extracted several times with dichloromethane until the pH of the aqueous phase remained basic. The organic fractions were collected together, treated with Na$_2$SO$_4$, and dried, affording 229.3 mg (0.52 mmol, 80% yield) of a white solid. ^{1}H NMR (400 MHz, Chloroform-*d*) δ 7.87 (dd, J = 7.0, 1.8 Hz, 2H), 7.64 (m, 4H), 4.44 (m, 4H), 3.97 (m, 4H), 2.81 (td, J = 10.3, 4.1 Hz, 1H), 2.54 (s, 3H), 2.34 (ddd, J = 11.5, 9.8, 3.4 Hz, 1H), 2.13 – 1.90 (m, 2H), 1.84 – 1.75 (m, 1H), 1.68 – 1.59 (m, 1H), 1.41 (t, J = 7.1 Hz, 6H), 1.20 (m, 2H). ^{13}C NMR (101 MHz, Chloroform-*d*) δ 165.42, 161.15, 147.73, 137.20, 126.14, 123.32, 67.54, 61.89, 56.45, 52.12, 34.92, 25.76, 25.11, 24.05, 14.44. MS (ESI$^+$, MeOH/H$_2$O): m/z; 441.111 calculated for [C$_{24}$H$_{33}$N$_4$O$_4$]$^+$ 441.2496.

6,6′-(((*trans*-2-(bis(carboxymethyl)amino)cyclohexyl) azanediyl)bis(methylene))dipicolinic acid (H$_4$*CHX*OITAPA). *tert*-Butyl 2-bromoacetate (80 µL, 0.54 mmol) was added to a suspension of **4** (119.4 mg, 0.270 mmol) and K$_2$CO$_3$ (299.0 mg, 2.16 mmol) in acetonitrile (20 mL), and the mixture was left stirring at room temperature during 14 days. After this time, the excess of K$_2$CO$_3$ was removed by filtration, 50 mL of water was added, and the mixture was extracted with 4×25 mL of dichloromethane. The organic fractions were collected together, treated with Na$_2$SO$_4$, and evaporated under reduced pressure, affording a yellow oil. This was finally treated with 20 mL of 6 M HCl, and the mixture was refluxed for 12 h. The crude was purified by MPLC using a reverse phase C18AQ (20 g) column and H$_2$O (0.1% TFA) / CH$_3$CN (0.1% TFA) as mobile phase. The ligand eluted at 37% of CH$_3$CN (0.1% TFA), affording a white solid (37% yield, 69.7 mg, 0.10 mmol). ^{1}H NMR (400 MHz, Deuterium Oxide) δ 7.97 (m, 6H), 4.23 (d, J = 14.1 Hz, 2H), 3.52 (d, J = 15.8 Hz, 2H), 3.35 (m, 2H), 2.27 (d, J = 12.3 Hz, 1H), 2.05 (d, J = 11.6 Hz, 1H), 1.78 (m, 2H), 1.50 (m, 1H), 1.27 (m, 2H). ^{13}C NMR (101 MHz, Deuterium Oxide) δ 170.23, 129.04, 125.15, 62.84, 62.05, 24.22, 24.06, 23.74, 23.52. MS (ESI$^+$, MeOH/H$_2$O): m/z 501.1982; calculated for [C$_{24}$H$_{29}$N$_4$O$_8$]$^+$ 501.1980. Elemental analysis calcd (%) for C$_{24}$H$_{24}$N$_4$O$_8$ ·1.7TFA: C 47.40, H 4.31, N 8.07; found: C 47.83, H 4.19, N 7.80.

Crystal Structure Determination: Single crystals with formula [Y(H*CHX*OICTAPA)(H$_2$O)]·2H$_2$O were obtained from an acidified aqueous solution of the complex and analysed by X-ray diffraction. Crystallographic data and the structure refinement parameters are given in Table S3). Measurements were performed at 100 K on a Bruker D8 Venture diffractometer with a Photon 100 CMOS detector and Mo-Kα radiation (λ = 0.71073 Å) generated by an Incoatec high brillance microfocus source equipped with Incoatec Helios

multilayer optics. The software APEX4[53] was used for collecting frames of data, indexing reflections, and the determination of lattice parameters, while SAINT[54] was used for integrating the intensity of reflections, and SADABS[55] for scaling and empirical absorption correction. The structure was solved by dual-space methods using the program SHELXT.[56] All non-hydrogen atoms were refined with anisotropic thermal parameters by full-matrix least-squares calculations on F2 using the program SHELXL-2014.[57] Hydrogen atoms were inserted at calculated positions and constrained with isotropic thermal parameters.

Deposition Number 2427211 contains the supplementary crystallographic data for this paper. These data are provided free of charge by the joint Cambridge Crystallographic Data Centre and Fachinformationszentrum Karlsruhe Access Structures service.

Potentiometric and Relaxometric Titrations: The protonation constants of the *CHX*OITAPA^{4-} ligand were determined by using a Metrohm 888 Titrando instrument equipped with a Metrohm 6.0234.100 combined glass electrode. For the two-point calibration prior to the titrations, KH-phthalate (pH = 4.002) and borax (pH = 9.177) standard buffers were used. The titrated sample (5.00 mL, 2.51 mM ligand) was continuously stirred and thermostated (25 °C) under an inert atmosphere (N_2) to avoid the effect of CO_2. The ionic strength in the samples was set to 0.15 M by NaCl. The concentrations of the H^+ were calculated from the measured pH values by applying the method proposed by Irving et al.[58] A solution of ≈0.02 M HCl was titrated with a 0.15 M NaOH solution (0.15 M NaCl), and the differences between the measured and calculated pH values (for the points with pH < 2.2) were used to calculate the [H^+] from the pH values measured in the titration experiments. The measured points with pH > 11.0 of the acid-base titration were used to calculate the ionic product of the water, which was found to be 13.856 (0.15 M NaCl) under the experimental conditions applied. The pH potentiometric titration curves were measured in the pH range of 1.85 – 11.85. For the calculation of the equilibrium constants, the PSEQUAD program was used.[59]

Due to the high stability of the Ln^{3+} complexes, the relaxometric method was applied for the determination of stability constants by measuring the longitudinal ($1/T_1$) and transverse ($1/T_2$) relaxation rates of the samples using Bruker Minispec MQ-20 and MQ-60 NMR instruments. The longitudinal relaxation times were measured by the inversion-recovery method (180° − τ − 90°), averaging 5−6 data points for each sample obtained at 10 different τ values. The transversal relaxation times were determined by using the Carr-Purcell-Meiboom-Gill pulse sequence,[60] by averaging 5–6 identical readouts. The samples were thermostated at 25.0 °C by using a circulating water bath. The stability of Gd^{3+} complex was determined using batch samples (9 samples) in the range of complex formation in acidic conditions (pH_{calc} = 1.058 – 1.930). The samples were prepared using constant ligand and Gd^{3+} concentrations (c_L = 1.43 mM and $c_{Gd^{3+}}$ = 1.50 mM). The transmetalation reactions were also followed by relaxometry using the batch method. In these samples, the Gd^{3+}:ligand ratio was 1:1, and the concentrations of Y^{3+} or Lu^{3+} were increased until the exchange of the paramagnetic Gd^{3+} by the diamagnetic counterpart was evidenced. The specific conditions used were for Y^{3+}:[Gd^{3+}] = 1.52 mM, [L] = 1.49 mM, pH 4.59, 0.05 M DMP buffer, and for Lu^{3+}: [Gd^{3+}] = 1.25 mM, [L] = 1.30 mM pH 4.57, 0.05 M DMP buffer.

Kinetic Studies: The rates of the metal exchange reactions involving the [Y(*CHX*OITAPA)]$^-$ and [Lu(*CHX*OITAPA)]$^-$ complexes and Cu^{2+} were studied by using UV–vis spectrophotometry following the formation of the [Cu_2(*CHX*OITAPA)] complex. The conventional UV−vis spectroscopic method was applied to follow the transmetalation reactions, as these reactions were very slow under the conditions applied (in the pH range of 3.60−4.81). Absorbance versus time kinetic curves were acquired by using a Jasco V-770 UV–vis−NIR spectrophotometer equipped with a Peltier thermostated multicell holder. The temperature was maintained at 25 °C, and the ionic strength of the solutions was kept constant by using 0.15 M NaCl. For keeping the pH constant, 50 mM DMP buffer was used (log K_2^H = 4.19(5) as determined by using pH-potentiometry at 25 °C with the use of 0.15 M NaCl ionic strength). The exchange reactions were followed continuously at 310 nm for 3−4 days (80−95% conversion) and occasionally (one or two readouts per day) for another 5–7 days. The absorbance readings at equilibrium were determined 3−4 weeks after the start of the reaction, depending on the pH of the samples (a time point being 8−10 times the half-life of the reaction). The concentration of the [Y(*CHX*OITAPA)]$^-$ chelate was 0.398 mM, whereas in the case of [Lu(*CHX*OITAPA)]$^-$ it was 0.302 mM, while the Cu^{2+} ion was applied at a high excess of ≈11–41 fold in order to ensure pseudo-first-order conditions. The pseudo-first-order rate constants (k_{obs}) were calculated by fitting the absorbance−time data with the computer program Micromath Scientist, version 2.0 (Salt Lake City, UT, USA) by using a standard least-squares procedure.

DFT Calculations: The geometries of the Y^{3+} complexes were optimized using DFT calculations with the Gaussian 16 program package,[61] using the M062X[62] functional and the 6–311G(d,p) basis set for the ligand atoms. The ECP28MWB quasi-relativistic effective core potential of Andrae et al. and its associated (8s7p6d)/[6s5p3d]-GTO valence basis set was used for Y.[63] Bulk water solvent effects were considered with the polarized continuum model (PCM), using the integral equation formalism variant.[64,65] Frequency calculations confirmed the nature of the optimized geometries as stationary points. An ultrafine integration grid was used throughout.

^{89}Y NMR shielding tensors were calculated with the ORCA suite (version 6.0.0),[66–68] which employs the SHARK integral package,[69] using the TPSSh functional.[70] Scalar relativistic effects were taken into account with the Zeroth Order Regular Approximation (ZORA)[71] method, using the SARC-ZORA-TZVPP basis set for Y and the all-electron ZORA-Def2-TZVPP basis set for the ligand atoms.[72,73] Shielding tensors were calculated with the gauge-including atomic orbitals (GIAO)[74] method and the resolution of identity and chain of spheres exchange (RIJCOSX)[75–78] approximation, using the def2/J and SARC/J auxiliary basis sets.[79] The DFT and COSX grids were set with the DefGrid3 keyword. Solvent effects were incorporated with a continuum model of the solvent defined by the bulk dielectric constant and atomic surface tensions (SMD).[80]

Radiolabeling: Yttrium-90 chloride ([^{90}Y]YCl_3) and no-carrier-added lutetium-177 chloride ([^{177}Lu]$LuCl_3$), in a 0.04 M HCl solution, were provided respectively by Eckert & Ziegler Radiopharma GmbH (Berlin, Germany) and ITM Medical Isotopes GmbH (Garching, Germany). Deionized water (≥18 MΩ cm) was obtained from a Milli-Q Reference water purification system. Human serum, issued from a pool of donors, was provided by Biopredic (Saint-Grégoire, France). Other chemicals (solvents, buffer solutions) were purchased from Sigma-Aldrich (Saint–Louis, Mo, USA) and used as received. Buffers were rendered metal-free by contact with Chelex (5 g L^{-1}) overnight. Activities were measured with a CRC-55tR (Capintec Inc., Ramsey, NJ, USA) dose calibrator. Radiochemical yields (RCY) were determined via radio-TLC by spotting an aliquot (5 µL) of the reaction solution onto instant thin layer chromatography-silica gel (iTLC-SG) strips (Agilent, Folsom, CA, USA), eluted in NaOH 10 mM/NaCl and subsequent measurement with a Cyclone Storage Phospho-

rimager (PerkinElmer, Waltham, MA, USA), using the Optiquant software. HPLC analyses were performed on HPLC Dionex Ultimate 3000 (Sunnyvale, CA, USA) equipped with a diode array detector and a radiochromatographic *f*Lumo (Berthold Technologies GmbH, Bad Wildbad, Germany) detector piloted by the Chromeleon software. The chromatographic analytic system employs a Phenomenex Luna C18(2) 250×4.6 mm, 5 µm column with A = H_2O 0.1% TFA; B = Acetonitrile as eluents; 0–20 min: 0–100% B, 20–25 min: 100% A, at a flow rate of 1 mL min^{-1}.

Radiolabeling experiments with $[^{90}Y]Y^{3+}$ and $[^{177}Lu]Lu^{3+}$ were performed in duplicate at each chelator concentration by addition of varying volumes of a solution of the chelator in water (5–50 µL; 0.01–1 mg mL^{-1}) and the radionuclide working solution (10 µL; 10–50 MBq ^{90}Y, 20–40 MBq ^{177}Lu) to 1.5-mL capped polypropylene tubes containing 10 mM acetate buffers (4.5-7; to reach a final volume of 1 mL), giving a final chelator concentration of 2.10^{-7}–10^{-4} M. The samples were shaken to ensure complete mixing and then incubated at room temperature for 10 min.

For the stability study in human serum, aliquots (0.2 mL) of the radiocomplex solutions prepared under an optimized procedure were mixed with 1 mL of human serum. The mixture was incubated at 37 °C under slight stirring. A 100 µL aliquot was taken and, after denaturing serum proteins with an equal amount of absolute ethanol and centrifugation (3500 g, 4 °C, 15 min), the supernatant was analyzed on radio-TLC (iTLC-SG strips eluted in EDTA 50 mM/H_2O) after 24, 48, 72 and 144 h for ^{90}Y, and up to 240 for ^{177}Lu. Each sample has been analyzed in triplicate.

Acknowledgements

D.E.-G. and C.P.-I. thank Ministerio de Ciencia e Innovación (Grant PID2022-138335NB-I00) and Xunta de Galicia (ED431C 2023/33) for generous financial support, as well as Centro de Supercomputación de Galicia (CESGA) for providing access to supercomputer facilities. P. P.-L. is indebted to CACTI (Universidade de Vigo) for X-ray measurements. The research was funded by the Hungarian National Research, Development and Innovation Office (NKFIH K-134694 project) and implemented with the support of the University of Debrecen's Publication Support Programme. B.Sz. was supported by the Doctoral School of Chemistry at the University of Debrecen, Hungary. N.L. acknowledges support by Labex Iron (grant no. ANR-11-LABX-0018). This work has been carried out within the framework of the Coordinated Research Project F22078 organized by the International Atomic Energy Agency (IAEA).

Conflict of Interests

The authors declare no conflict of interest.

Data Availability Statement

The data that support the findings of this study are available from the corresponding author upon reasonable request.

Keywords: ligands · lutetium · radiopharmaceuticals · thermodynamics · yttrium

[1] C. Platas-Iglesias, M. Mato-Iglesias, K. Djanashvili, R. N. Muller, L. V. Elst, J. A. Peters, A. de Blas, T. Rodríguez-Blas, *Chem. – Eur. J.* **2004**, *10*, 3579.
[2] N. Chatterton, C. Gateau, M. Mazzanti, J. Pécaut, A. Borel, L. Helm, A. Merbach, *Dalton Trans.* **2005**, 1129.
[3] F. Lucio-Martínez, Z. Garda, B. Váradi, F. K. Kálmán, D. Esteban-Gómez, É. Tóth, G. Tircsó, C. Platas-Iglesias, *Inorg. Chem.* **2022**, *61*, 5157.
[4] E. W. Price, J. F. Cawthray, G. A. Bailey, C. L. Ferreira, E. Boros, M. J. Adam, C. Orvig, *J. Am. Chem. Soc.* **2012**, *134*, 8670.
[5] F. K. Kálmán, A. Végh, M. Regueiro-Figueroa, É. Tóth, C. Platas-Iglesias, G. Tircsó, *Inorg. Chem.* **2015**, *54*, 2345.
[6] M. de G Jaraquemada-Peláez, X. Wang, T. J. Clough, Y. Cao, N. Choudhary, K. Emler, B. O. Patrick, C. Orvig, *Dalton Trans.* **2017**, *46*, 14647.
[7] G. Tircsó, M. Regueiro-Figueroa, V. Nagy, Z. Garda, T. Garai, F. K. Kálmán, D. Esteban-Gómez, É. Tóth, C. Platas-Iglesias, *Chem. – Eur. J.* **2016**, *22*, 896.
[8] C. F. Ramogida, J. F. Cawthray, E. Boros, C. L. Ferreira, B. O. Patrick, M. J. Adam, C. Orvig, *Inorg. Chem.* **2015**, *54*, 2017.
[9] F. Lucio-Martínez, D. Esteban-Gómez, L. Valencia, D. Horváth, D. Szücs, A. Fekete, D. Szikra, G. Tircsó, C. Platas-Iglesias, *Chem. Commun.* **2023**, *59*, 3443.
[10] T. I. Kostelnik, C. Orvig, *Chem. Rev.* **2019**, *119*, 902.
[11] M. Van De Voorde, K. Van Hecke, T. Cardinaels, K. Binnemans, *Coord. Chem. Rev.* **2019**, *382*, 103.
[12] L. Li, M. De Guadalupe Jaraquemada-Peláez, E. Aluicio-Sarduy, X. Wang, T. E. Barnhart, W. Cai, V. Radchenko, P. Schaffer, J. W. Engle, C. Orvig, *Dalton Trans.* **2020**, *49*, 5547.
[13] S. M. Qaim, *Nucl. Med. Biol.* **2017**, *44*, 31.
[14] A. Dash, M. R. A. Pillai, F. F. Knapp, *Nucl. Med. Mol. Imaging* **2015**, *49*, 85.
[15] U. Hennrich, M. Eder, *Pharmaceuticals* **2022**, *15*, 1292.
[16] S. Banerjee, M. R. A. Pillai, F. F. Russ Knapp, *Chem. Rev.* **2015**, *115*, 2934.
[17] T. Ladrière, J. Faudemer, E. Levigoureux, D. Peyronnet, C. Desmonts, J. Vigne, *Pharmaceutics* **2023**, *15*, 1240.
[18] S. C. George, E. J. J. Samuel, *Front. Chem.* **2023**, *11*, 1218670.
[19] L. Wharton, H. Yang, M. D. G. Jaraquemada-Peláez, H. Merkens, G. Engudar, A. Ingham, H. Koniar, V. Radchenko, P. Kunz, P. Schaffer, F. Bénard, C. Orvig, *J. Med. Chem.* **2023**, *66*, 13705.
[20] A. Hu, I. Keresztes, S. N. MacMillan, Y. Yang, E. Ding, W. R. Zipfel, R. A. DiStasio, J. W. Babich, J. J. Wilson, *Inorg. Chem.* **2020**, *59*, 5116.
[21] R. Uzal-Varela, A. Rodríguez-Rodríguez, H. Wang, D. Esteban-Gómez, I. Brandariz, E. M. Gale, P. Caravan, C. Platas-Iglesias, *Coord. Chem. Rev.* **2022**, *467*, 214606.
[22] M. Regueiro-Figueroa, B. Bensenane, E. Ruscsák, D. Esteban-Gómez, L. J. Charbonnière, G. Tircsó, I. Tóth, A. de Blas, T. Rodríguez-Blas, C. Platas-Iglesias, *Inorg. Chem.* **2011**, *50*, 4125.
[23] Z. Baranyai, M. Botta, M. Fekete, G. B. Giovenzana, R. Negri, L. Tei, C. Platas-Iglesias, *Chem. – Eur. J.* **2012**, *18*, 7680.
[24] R. Negri, Z. Baranyai, L. Tei, G. B. Giovenzana, C. Platas-Iglesias, A. C. Bényei, J. Bodnár, A. Vágner, M. Botta, *Inorg. Chem.* **2014**, *53*, 12499.
[25] P. Lagriffoule, M. Eriksson, K. K. Jensen, P. E. Nielsen, P. Wittung, B. Nordén, O. Buchardt, *Chem. – Eur. J.* **1997**, *3*, 912.
[26] R. Fornasier, D. Milani, P. Scrimin, U. Tonellato, *J. Chem. Soc. Perkin Trans. 2* **1986**, 233.
[27] S. Achilefu, R. R. Wilhelm, H. N. Jimenez, M. A. Schmidt, A. Srinivasan, *J. Org. Chem.* **2000**, *65*, 1562.
[28] A. Ruiz-Martínez, D. Casanova, S. Alvarez, *Chem. – Eur. J.* **2008**, *14*, 1291.
[29] J. Kotek, J. Rudovský, P. Hermann, I. Lukeš, *Inorg. Chem.* **2006**, *45*, 3097.
[30] D. Parker, K. Pulukkody, F. C. Smith, A. Batsanov, J. A. K. Howard, *J. Chem. Soc. Dalton Trans.* **1994**, 689.
[31] K. Kumar, C. A. Chang, L. C. Francesconi, D. D. Dischino, M. F. Malley, J. Z. Gougoutas, M. F. Tweedle, *Inorg. Chem.* **1994**, *33*, 3567.
[32] E. Kriemen, M. Holzapfel, E. Ruf, J. Rehbein, W. Maison, *Eur. J. Inorg. Chem.* **2015**, *2015*, 5368.
[33] W.-Y. Hsieh, S. Liu, *Inorg. Chem.* **2004**, *43*, 6006.
[34] M. Le Fur, M. Beyler, E. Molnár, O. Fougère, D. Esteban-Gómez, G. Tircsó, C. Platas-Iglesias, N. Lepareur, O. Rousseaux, R. Tripier, *Inorg. Chem.* **2018**, *57*, 2051.
[35] P. Vojtíšek, P. Cígler, J. Kotek, J. Rudovský, P. Hermann, I. Lukeš, *Inorg. Chem.* **2005**, *44*, 5591.
[36] Y. Xing, A. K. Jindal, M. Regueiro-Figueroa, M. Le Fur, N. Kervarec, P. Zhao, Z. Kovacs, L. Valencia, P. Pérez-Lourido, R. Tripier, D. Esteban-Gómez, C. Platas-Iglesias, A. D. Sherry, *Chem. – Eur. J.* **2016**, *22*, 16657.

[37] R. D. Shannon, *Acta Crystallogr. A* **1976**, *32*, 751.
[38] A. A. B. Baloch, S. M. Alqahtani, F. Mumtaz, A. H. Muqaibel, S. N. Rashkeev, F. H. Alharbi, *Phys. Rev. Mater.* **2021**, *5*, 043804.
[39] C. Harriswangler, J. C. Frías, M. T. Albelda, L. Valencia, E. García-España, D. Esteban-Gómez, C. Platas-Iglesias, *Inorg. Chem.* **2023**, *62*, 17030.
[40] S. K. Wolff, T. Ziegler, E. Van Lenthe, E. J. Baerends, *J. Chem. Phys.* **1999**, *110*, 7689.
[41] G. Castro, G. Wang, T. Gambino, D. Esteban-Gómez, L. Valencia, G. Angelovski, C. Platas-Iglesias, P. Pérez-Lourido, *Inorg. Chem.* **2021**, *60*, 1902.
[42] E. W. Price, J. F. Cawthray, M. J. Adam, C. Orvig, *Dalton Trans.* **2014**, *43*, 7176.
[43] G. Anderegg, F. Arnaud-Neu, R. Delgado, J. Felcman, K. Popov, *Pure Appl. Chem.* **2005**, *77*, 1445.
[44] A. Forgács, M. Regueiro-Figueroa, J. L. Barriada, D. Esteban-Gómez, A. De Blas, T. Rodríguez-Blas, M. Botta, C. Platas-Iglesias, *Inorg. Chem.* **2015**, *54*, 9576.
[45] A. Vágner, C. D'Alessandria, G. Gambino, M. Schwaiger, S. Aime, A. Maiocchi, I. Tóth, Z. Baranyai, L. Tei, *ChemistrySelect* **2016**, *1*, 163.
[46] D. H. Powell, O. M. N. Dhubhghaill, D. Pubanz, L. Helm, Y. S. Lebedev, W. Schlaepfer, A. E. Merbach, *J. Am. Chem. Soc.* **1996**, *118*, 9333.
[47] W. R. Harris, K. N. Raymond, F. L. Weitl, *J. Am. Chem. Soc.* **1981**, *103*, 2667.
[48] K. J. Powell, P. L. Brown, R. H. Byrne, T. Gajda, G. Hefter, S. Sjöberg, H. Wanner, *Pure Appl. Chem.* **2007**, *79*, 895.
[49] J. Martinelli, E. Romano, A. Laczovics, D. Horváth, E. Grattoni, Z. Baranyai, L. Tei, *Chem. – Eur. J.* **2024**, *30*, e202400570.
[50] D. Ndiaye, M. Sy, W. Thor, L. J. Charbonnière, A. M. Nonat, É. Tóth, *Chem. – Eur. J.* **2023**, *29*, e202301880.
[51] R. F. W. Bader, M. T. Carroll, J. R. Cheeseman, C. Chang, *J. Am. Chem. Soc.* **1987**, *109*, 7968.
[52] E. W. Price, B. M. Zeglis, J. F. Cawthray, J. S. Lewis, M. J. Adam, C. Orvig, *Inorg. Chem.* **2014**, *53*, 10412.
[53] APEX4, *Bruker AXS Inc*, Madison, Wisconsin, USA **2021**.
[54] *SAINT Version 8.37A; Bruker AXS Inc*., Madison, Wisconsin, USA **2015**.
[55] G. M. Sheldrick, **2014**.
[56] G. M. Sheldrick, *Acta Crystallogr. Sect. C Struct. Chem.* **2015**, *71*, 3.
[57] G. M. Sheldrick, *Acta Crystallogr. A* **2008**, *64*, 112.
[58] H. M. Irving, M. G. Miles, L. D. Pettit, *Anal. Chim. Acta* **1967**, *38*, 475.
[59] (Ed: D. J. Leggett), *Computational Methods for the Determination of Formation Constants*, Springer US, Boston, MA, **1985**.
[60] S. Meiboom, D. Gill, *Rev. Sci. Instrum.* **1958**, *29*, 688.
[61] M. J. Frisch, G. W. Trucks, H. B. Schlegel, G. E. Scuseria, M. A. Robb, J. R. Cheeseman, G. Scalmani, V. Barone, G. A. Petersson, H. Nakatsuji, X. Li, M. Caricato, A. V. Marenich, J. Bloino, B. G. Janesko, R. Gomperts, B. Mennucci, H. P. Hratchian, J. V. Ortiz, A. F. Izmaylov, J. L. Sonnenberg, F. D. Williams, F. Lipparini, F. Egidi, J. Goings, B. Peng, A. Petrone, T. Henderson, D. Ranasinghe, V. G. Zakrzewski, et al., *Gaussian 16 Rev. C.01*, Wallingford, CT, **2016**.
[62] Y. Zhao, D. G. Truhlar, *Theor. Chem. Acc.* **2008**, *120*, 215.
[63] D. Andrae, U. Häussermann, M. Dolg, H. Stoll, H. Preuss, *Theor. Chim. Acta* **1990**, *77*, 123.
[64] E. Cancès, B. Mennucci, J. Tomasi, *J. Chem. Phys.* **1997**, *107*, 3032.
[65] J. Tomasi, B. Mennucci, R. Cammi, *Chem. Rev.* **2005**, *105*, 2999.
[66] F. Neese, *WIREs Comput. Mol. Sci.* **2012**, *2*, 73.
[67] F. Neese, *WIREs Comput. Mol. Sci.* **1327**, *2018*, 8, e.
[68] F. Neese, F. Wennmohs, U. Becker, C. Riplinger, *J. Chem. Phys.* **2020**, *152*, 224108.
[69] F. Neese, *J. Comput. Chem.* **2023**, *44*, 381.
[70] J. Tao, J. P. Perdew, V. N. Staroverov, G. E. Scuseria, *Phys. Rev. Lett.* **2003**, *91*, 146401.
[71] C. Van Wüllen, *J. Chem. Phys.* **1998**, *109*, 392.
[72] F. Weigend, R. Ahlrichs, *Phys. Chem. Chem. Phys.* **2005**, *7*, 3297.
[73] R. Julian D, F. Neese, D. A. Pantazis, *J. Comput. Chem.* **2020**, *41*, 1842.
[74] G. L. Stoychev, A. A. Auer, R. Izsák, F. Neese, *J. Chem. Theory Comput.* **2018**, *14*, 619.
[75] F. Neese, F. Wennmohs, A. Hansen, U. Becker, *Chem. Phys.* **2009**, *356*, 98.
[76] B. Helmich-Paris, B. De Souza, F. Neese, R. Izsák, *J. Chem. Phys.* **2021**, *155*, 104109.
[77] R. Izsák, F. Neese, *J. Chem. Phys.* **2011**, *135*, 144105.
[78] R. Izsák, F. Neese, W. Klopper, *J. Chem. Phys.* **2013**, *139*, 094111.
[79] F. Weigend, *Phys. Chem. Chem. Phys.* **2006**, *8*, 1057.
[80] A. V. Marenich, C. J. Cramer, D. G. Truhlar, *J. Phys. Chem. B* **2009**, *113*, 6378.

Manuscript received: February 28, 2025
Revised manuscript received: March 27, 2025
Version of record online: April 24, 2025